

1 The location of the Earth's magnetopause: a
2 comparison of modeled position and in-situ Cluster
3 data

N. A. Case¹ and J. A. Wild¹

Space Plasma Environment and Radio Science Group, Department of Physics, Lancaster University, Lancaster, LA1 4YB, UK (n.case@lancaster.ac.uk)

¹Department of Physics, Lancaster University, Lancaster, UK.

4 **Abstract.** Exploiting eight years of magnetic field data from the Clus-
5 ter mission, we employ an automated magnetopause crossing detection rou-
6 tine to determine the magnetopause location over varying magnetic latitude
7 and local time. For a period spanning nearly one solar cycle we build a database
8 of 2709 magnetopause crossings and compare these locations to the magne-
9 topause models of *Petrinec and Russell* [1996], *Shue et al.* [1998], *Dmitriev*
10 *and Suvorova* [2000] and *Lin et al.* [2010]. We compare our detected loca-
11 tions with the predicted locations for a variety of solar wind conditions and
12 positions on the magnetopause. We find that, on average, the *Petrinec and*
13 *Russell* [1996] and *Shue et al.* [1998] models overestimate the radial distance
14 to the magnetopause by $\sim 1 R_E$ (9%) whilst the *Dmitriev and Suvorova* [2000]
15 and *Lin et al.* [2010] models underestimate it by $0.5 R_E$ (4.5%) and $0.25 R_E$
16 (2.3%) respectively. Some varying degree of control on the differences between
17 the predicted and encountered locations, by the solar wind and location pa-
18 rameters, are found.

1. Introduction

19 The accurate determination of the size and configuration of the magnetosphere is acutely
20 important when investigating interactions between the interplanetary and near-Earth
21 space environments. Understanding how the solar wind and interplanetary magnetic
22 field (IMF) constrains the Earth's magnetosphere requires accurate specification of the
23 magnetopause location under a variety of conditions.

24 *Chapman and Ferraro* [1931] first introduced the concept of a magnetopause whose
25 shape and size is dependent upon the solar wind dynamic pressure (P_d). Since then,
26 several empirical models have been developed to describe the shape and location of the
27 magnetopause based on *in situ* satellite measurements. Examples include *Fairfield* [1971],
28 *Roelof and Sibeck* [1993], *Petrinec and Russell* [1996], *Shue et al.* [1997] and *Suворova et al.*
29 [1999]. The accuracy of such models can be assessed further by comparing the predicted
30 magnetopause position with spacecraft observations of the boundary not included in the
31 original modelling process (e.g. *Shue et al.* [1998], *Šafránková et al.* [2002] and *Dmitriev*
32 *et al.* [2011]).

33 Although it is possible to survey the magnetopause location via changes in the ob-
34 served magnetic field and plasma characteristics at a spacecraft, the boundary can vary
35 in thickness from around 400-700 km [*Berchem and Russell*, 1982] and, depending upon
36 a spacecraft's trajectory, it may pass through the boundary rapidly (\sim seconds) or skim
37 along the magnetopause passing in and out in multiple times in quick succession over a
38 longer period (\sim hours).

39 Manual determination of a magnetopause crossing can be a labor-intensive task requir-
40 ing the identification of discontinuities in magnetic field data, plasma data or both. In
41 a large scale survey, with hundreds or thousands of potential crossings, this can become
42 impractical and an effective automated routine is desirable. Such an automated method
43 would need to exploit a clearly-defined set of criteria to determine what physical paramete-
44 r changes constitute a boundary crossing event over an appropriate spatial and temporal
45 timescale.

46 In this study, a modified version of the *Ivchenko et al.* [2000] automated magnetopause
47 crossing routine is applied to ~ 8 years of magnetic field data from the Cluster mission to
48 determine the location of the magnetopause. The detected crossings locations are then
49 compared to the commonly-used magnetopause models of *Petrinec and Russell* [1996],
50 *Shue et al.* [1998], *Dmitriev and Suvorova* [2000] and *Lin et al.* [2010].

51 *Petrinec and Russell* [1996] presents a cylindrically symmetrical empirical magnetopause
52 model based on data from the ISEE satellite missions [*Song et al.*, 1988] and is an amal-
53 gamation of two earlier models: *Petrinec et al.* [1991] and *Petrinec and Russell* [1993].
54 *Petrinec et al.* [1991] modeled the dayside magnetopause using a best fit ellipsoid function
55 to ISEE 1 and 2 magnetopause crossings; *Petrinec and Russell* [1993] used magnetic pres-
56 sure balancing of the magnetopause to infer the location of the magnetotail. *Petrinec and*
57 *Russell* [1996] then combine these two models with a smooth connection at the terminator.

58 The *Petrinec and Russell* [1996] model ignores nonaxisymmetric functions on the day-
59 side magnetopause (including the magnetic cusp regions). It has a range of validity for the
60 input parameters of $-10 < B_z < 10$ nT and $0.5 < P_d < 8$ nPa and has different modeling
61 parameter values based upon the orientation of B_z .

62 The *Shue et al.* [1998] model is an improved version of the earlier *Shue et al.* [1997]
63 model which was derived as an empirical best fit to data from several magnetospheric
64 satellites, including ISEE 1 & 2 and IMP 8. After further testing with a magnetic cloud
65 event in 1997, in which the magnetopause passed inside geosynchronous orbit, *Shue et al.*
66 [1998] improved the functional forms of the *Shue et al.* [1997] model to better represent
67 the effect of P_d on the flaring angle and of B_z on the subsolar standoff distance. As with
68 *Petrinec and Russell* [1996], the *Shue et al.* [1998] model is cylindrically symmetric and
69 does not account for the magnetospheric cusp regions.

70 The previous two models are both 2-dimensional and empirically derived using two input
71 parameters: the magnetic field component B_z and the solar wind dynamic pressure (P_d)
72 as these two parameters have been found to be significant in modeling the magnetopause
73 location by many previous studies (e.g. *Petrinec et al.* [1991], *Sibeck et al.* [1991] and *Roelof*
74 *and Sibeck* [1993]). *Dmitriev and Suvorova* [2000], however, used an Artificial Neural
75 Network (ANN) to develop a complex, multi-parameter, 3-D model of the magnetopause.

76 *Dmitriev and Suvorova* [2000] employ the selection criteria developed by Kuznetsov
77 and Suvorova [1997] on dayside magnetopause crossings from *Roelof and Sibeck* [1993]
78 and geosynchronous crossings from Kuznetsov and Suvorova [1997] to build a data set
79 of 999 magnetopause crossings (assuming a mirrored symmetry in the ecliptic plane) to
80 input into the ANN model. Initially, 30 different parameters were included in the model,
81 however, *Dmitriev and Suvorova* [2000] were able to reduce the number of required inputs
82 to five parameters (λ - the GSE latitude, φ - the GSE longitude, B_y (GSM), B_z (GSM)
83 and $\ln[P_d]$) whilst keeping a model correlation accuracy of 0.92 and a standard deviation of

84 1.04 R_E [Dmitriev and Suvorova, 2000]. The [Dmitriev and Suvorova, 2000] is asymmetric
85 in the dawn-dusk plane.

86 With the ANN model there are several validity ranges on the input parameters, which
87 *Dmitriev and Suvorova* [2000] state should keep the relative error under 10%. The longi-
88 tude and latitude (GSE) should be between ± 90 degrees and ± 80 degrees respectively.
89 The magnetic field components should be between: $-20 < B_y < 20$ nT and $-20 < B_z$
90 < 20 nT and the dynamic pressure should be between $0.5 < P_d < 40$ nPa.

91 *Lin et al.* [2010] present a three-dimensional asymmetric magnetopause model which is
92 built upon the *Shue et al.* [1997] magnetopause model. In addition to exploiting the solar
93 wind dynamic pressure and the B_z component of the IMF as model parameters, the *Lin*
94 *et al.* [2010] model also takes into account the solar wind magnetic pressure (P_m) and the
95 Earth's magnetic dipole tilt angle (ϕ).

96 The *Lin et al.* [2010] model was developed using 980 magnetopause crossings from a
97 range of satellite missions (including Geotail, IMP and Cluster) with 5 minute averaged
98 solar wind parameters and 1482 Hawkeye magnetopause crossings with hourly solar wind
99 parameters. Using the Levenberg-Marquardt method for non-linear multi-parameter fit-
100 ting, *Lin et al.* [2010] determine the important control parameters for the magnetopause
101 size and shape and the relationships between them.

102 Unlike most magnetopause models, including *Petrinec and Russell* [1996] and *Shue et*
103 *al.* [1998], the *Lin et al.* [2010] model is able to account for the north-south asymmetry of
104 the magnetopause and for the indentations near the magnetic cusps and so should provide
105 more accurate results in these regions.

106 In the sections that follow, we discuss how we utilize the *in situ* magnetic field data
107 and how we modify the *Ivchenko et al.* [2000] magnetopause crossing detection routine
108 to determine the location of the magnetopause for eight years of satellite data. We then
109 compare our results to the models previously described.

2. In situ magnetic field data

110 The four European Space Agency (ESA) Cluster spacecraft have been in an elliptical
111 polar orbit around the Earth since 2000. During the northern hemisphere’s winter months
112 the spacecraft pass through the dayside magnetopause on their outward trajectory from
113 perigee to apogee. Over the mission lifetime, the orbital configuration has varied resulting
114 in encounters with the magnetopause over a wide range of latitudes and at varying local
115 times, due to the Earth’s orbit about the Sun. The wide range of latitudes accessible to
116 Cluster is in contrast to some earlier studies (e.g. *Ivchenko et al.* [2000] and *Dušík et al.*
117 [2010]) that focussed on spacecraft measurements at low latitudes.

118 The magnetic field data are collected by each spacecraft’s FGM instrument which con-
119 sists of two three-axis fluxgate magnetometers [*Gloag et al.*, 2010]. The FGM data used
120 in this study are obtained from the Cluster Active Archive (see *Laakso et al.* [2010]) at
121 four second resolution and are presented in this paper in the GSM co-ordinate system.
122 Magnetic field data are used exclusively, rather than in combination with plasma data, as
123 they are one of the most commonly available spacecraft data sets (both for Cluster and
124 other missions).

125 Solar wind data, which are required as an input into the models, are obtained from the
126 OMNIweb service (<http://omniweb.gsfc.nasa.gov>) at one minute resolution and are then
127 averaged to five minute resolution, as in *Shue et al.* [1997]. This “High Resolution OMNI”

128 data set contains an interspersal of ACE, Wind, IMP 8 and Geotail data which have been
129 time-shifted to the bow shock nose. The solar wind data are averaged to five minute
130 resolution since it is unclear how quickly the magnetopause responds to changing solar
131 wind conditions and the averaging also removes any ambiguity due to the lagging process.
132 Additionally, propagation times across the magnetosheath are ~ 4 mins (e.g. Khan and
133 Cowley [1999] and *Wild et al.* [2009]) and so this averaged data is generally representative
134 of the conditions at the magnetopause.

3. Methodology

135 We base our magnetopause crossing selection criteria on those of *Ivchenko et al.* [2000],
136 whose detection routine was applied to two and a half years of three-second resolution
137 magnetic field data from the Geotail mission. The four *Ivchenko et al.* [2000] criteria for
138 the determination of a crossing are:

- 139 1. the transition across the magnetopause should be completed within 30s;
- 140 2. the standard deviation of the magnetospheric magnetic field is required to be less
141 than 40% of the magnetic field on the magnetosheath side of the assumed boundary;
- 142 3. the northward component of the magnetospheric magnetic field is required to exceed
143 10 nT and;
- 144 4. the northward component of the magnetospheric magnetic field is required to be at
145 least a factor of 1.3 times greater than the corresponding magnetosheath component.

146 Since Geotail only encountered the magnetopause in a narrow range of latitudes, around
147 $\pm 2R_E$ from the GSM-x axis (typically in a skimming-type configuration) [Nishida, 1994],
148 whereas Cluster passes through the magnetopause at a range of latitudes, the *Ivchenko*
149 *et al.* [2000] criteria require modification. Specifically, *Ivchenko et al.* [2000] consider
150 the difference in the northward component of the magnetic field (B_z) either side of the
151 magnetopause boundary. This generally works well except in the following two cases: (1)
152 when the IMF is primarily orientated northward, in which case the B_z component of the
153 magnetic field is similar in both the magnetosheath and magnetosphere, and (2) at high
154 latitudes, where B_z tends to zero as the magnetic field is directed primarily toward/away
155 from the Earth (in the cusp region this changes with B_z once again becoming dominant
156 but now in the opposite direction). Case (1) is somewhat difficult to account for, but to
157 account for case (2): at high latitudes (where the angle between the spacecraft position
158 in the GSM x-y plane is greater than 45 degrees) we instead use the radial component of
159 the magnetic field (B_r).

160 Data from all four Cluster spacecraft between 2002-2010 are analyzed and, using the
161 modified *Ivchenko et al.* [2000] criteria, magnetopause crossings are detected. To reduce
162 data processing time, we focus on time intervals centered on the predicted magnetopause
163 crossings as given in the Cluster predicted events catalog [Hapgood *et al.*, 1997]. In order
164 to avoid a bias toward finding the magnetopause in close proximity to where the Cluster
165 planning software (which employs the *Sibeck et al.* [1991] magnetopause model) predicts
166 it will be located, we examine data from a four hour window. Over this window, the
167 spacecraft typically travel a distance of $\sim 5R_E$. We thus expect to capture virtually all
168 potential magnetopause crossings.

169 For determination of a magnetopause crossing, we employ a running average method
170 on the four hour window of magnetic field data. Two three minute segments of magnetic
171 field data, separated by a 32 second gap, are selected and tested against the following
172 modified *Ivchenko et al.* [2000] crossing criteria. If a crossing is not encountered then
173 the two segments of data chosen are shifted along in time by four seconds, however, if a
174 crossing is encountered then the segments chosen are shifted forward by 10 minutes. All
175 criteria must be met for a crossing to be determined.

176 1. The transition across the magnetopause boundary should be completed within
177 32 seconds (equivalent to eight spins of the Cluster spacecraft). The time of the cross-
178 ing event is recorded as when the spacecraft first crosses into the boundary layer and so
179 by enforcing this transition time limit we ensure that the recorded time of crossing is
180 accurate.

181 2. Multiple magnetopause crossings should not occur within 10 minutes. Multiple
182 crossings may occur when the spacecraft is skimming the magnetopause or when the
183 magnetopause location is rapidly fluctuating; rather than having multiple crossing events,
184 we instead choose the first event to represent the crossing location.

185 3. The standard deviation of the three minute window of magnetosheath magnetic field
186 must be greater than 4.5 on average and it must be a factor of 2.5 times larger than the
187 standard deviation of the three minute window of magnetospheric magnetic field. This
188 criteria requires that the magnetic field observed in the magnetosheath is fluctuating by
189 a larger amount than the magnetospheric magnetic field.

190 4. At low latitudes the B_z , and at high latitudes the B_r , component of the magneto-
191 spheric magnetic field must be greater than 10nT, since we take this to be a conservative
192 estimate of the minimum terrestrial magnetosphere field strength.

193 5. The particular magnetospheric magnetic field component, as determined by crite-
194 ria (4), must be a factor of at least 1.3 times greater the corresponding magnetosheath
195 magnetic field component. Although this may rule out occasions where the orientation of
196 the IMF is similar of that to the magnetosphere, this factor was determined to be most
197 appropriate in preventing small changes in the magnetic field from registering as crossing
198 events.

199 An example of a magnetopause encounter is shown in Figure 1. The three panels on the
200 left of the figure present magnetic field data from Cluster 1 showing the overall magnetic
201 field strength $|B|$, the appropriate magnetic field component (in this case B_r), the three
202 minute running standard deviation of $|B|$, and the clock angle of the measured magnetic
203 field, respectively. The clock angle is defined as the arctangent of the y-component of the
204 magnetic field over the z-component and is shown as measured at Cluster (yellow) and
205 the equivalent parameter predicted at the bowshock by OMNIweb (blue). The dashed
206 vertical black line in the left panel indicates the time at which the Cluster predicted events
207 catalog suggested a crossing would occur; the dashed red line indicates the time at which
208 the automated routine detected a crossing. The panel on the right of the figure shows the
209 Cluster spacecraft's position and a Tsyganenko-96 magnetic field model magnetosphere in
210 GSE co-ordinates. The modeled magnetosphere is determined for the time of the detected
211 crossing and is projected into the GSE X-Z plane (i.e. at $Y_{GSE} = 0$).

4. Results and Discussion

212 In total, 2709 crossings were detected using the automated routine described above,
 213 reducing to 2640 useful crossings due to missing/bad data in the OMNIweb database.
 214 This value is significantly less than 7418 predicted crossings listed in the predicted events
 215 catalog, however, this was to be expected since our selection criteria are somewhat con-
 216 servative.

217 The locations of these crossings are shown in Figure 2. The four panels in Figure 2
 218 represent different co-ordinate planes (from top left to bottom right): the noon-midnight
 219 meridian of the magnetosphere (with the Sun off to the left-hand side of the plot), a
 220 projection of the GSM equatorial plane from above the magnetic North Pole, a view of
 221 the Earth from the direction of the Sun and a projection of the radial distance to the
 222 magnetopause from the Earth as a function of X_{GSM} position.

223 Cluster's encounters with the magnetopause were detected over almost a full 180° range
 224 of latitudes with particularly high density regions at $\pm 10 R_E$ in the z-axis and over local
 225 times of 0900-1500 due to Cluster's orbital configuration.

226 The detected crossing locations were compared with the predicted magnetopause lo-
 227 cations for each of the four models discussed in the Introduction. The steps involved
 228 in calculating the radial separation distance (Δr) between the spacecraft location and
 229 the modeled magnetopause location are as follows. Firstly, we define the separation dis-
 230 tance as the radial location of the spacecraft subtracted from the radial location of the
 231 magnetopause:

$$\Delta r = r_{mp} - r_{sc} \quad (1)$$

232 where r_{sc} , the radial distance to the spacecraft, is defined as the length of the vector
 233 drawn from the Earth to the spacecraft location in the x- ρ plane:

$$r_{sc} = \sqrt{x_{sc}^2 + \rho^2} \quad (2)$$

234 where ρ is the length of the spacecraft position vector in the y-z plane:

$$\rho = \sqrt{y_{sc}^2 + z_{sc}^2} \quad (3)$$

235 and where r_{mp} is the radial distance to the modeled magnetopause, as determined indi-
 236 vidually for each model at spacecraft angle θ , the latitude in the x- ρ plane:

$$\theta = \arctan\left(\frac{\rho}{x_{sc}}\right) \quad (4)$$

237 where x_{sc} , y_{sc} and z_{sc} are the spacecraft's location in GSM x, y and z components.

238 Due to the validity limitations on the input parameters of the models we were able to
 239 compare 2599 crossings to the *Petrinec and Russell* [1996] model and 2621 crossings to the
 240 *Dmitriev and Suvorova* [2000] model. All 2640 crossings were compared against the *Shue*
 241 *et al.* [1998] and *Lin et al.* [2010] models since no parameter restrictions were specified.

242 Figure 3 compares the location of the *Petrinec and Russell* [1996] model magnetopause
 243 to the crossings detected by Cluster using the technique described above. The median
 244 difference in the radial location is found to be $1.06 R_E$, with the positive value indicating
 245 that the modelled magnetopause location is typically radially further from the Earth
 246 than the detected location. The histogram is generally symmetrically distributed about
 247 the median.

248 Figure 4 is a comparison between the *Shue et al.* [1998] model and our detected crossings.
 249 We find that the median difference is $1.48 R_E$, again indicating that the median modeled
 250 location was radially further out from the Earth than the detected location. The histogram

251 is symmetrical around the median, though with a greater spread than with the *Petrinec*
 252 *and Russell* [1996] model.

253 The detected crossing locations and the *Dmitriev and Suvorova* [2000] modeled magne-
 254 topause locations are compared in Figure 5. The median difference between the model and
 255 the detected crossing locations is $-0.52 R_E$, which, opposite to the previous two models,
 256 shows that the median modeled location was radially closer to the Earth than the detected
 257 crossing location. The difference distribution is non-symmetrical with a substantial tail,
 258 of approximately 250 (10%) events, at radial differences less than $-3 R_E$.

259 In Figure 6 the detected and predicted crossing locations are compared for the *Lin et al.*
 260 [2010] model. The median difference is $-0.24 R_E$ which, as with the *Dmitriev and Suvorova*
 261 [2000] model, suggests that, in general, the *Lin et al.* [2010] model slightly underestimates
 262 the distance to the magnetopause. The distribution of differences is similar to the *Dmitriev*
 263 *and Suvorova* [2000] distribution but with a smaller tail region (approximately 5% of
 264 events). Over half of the data lie within $\pm 1 R_E$.

265 The radial differences between the detected crossing locations and the four models are
 266 shown for four parameters (clock angle, B_z , P_d and θ) in Figure 7. The number of crossings
 267 are represented by the color-scaled density bins. The crosses indicate the median value
 268 for the row of bins and the error bars represent the standard deviation of the distribution
 269 in each row.

270 The clock angle has little or no influence on the radial difference for any of the models.
 271 There is little apparent relationship between the radial differences of the modeled and
 272 observed magnetopause locations and B_z for the *Petrinec and Russell* [1996] model. At
 273 $B_z < 4\text{nT}$, the radial differences for the *Shue et al.* [1998] model decrease from around $2 R_E$

274 to around $0 R_E$. The *Dmitriev and Suvorova* [2000] and *Lin et al.* [2010] model plots have
275 a similar form as the *Shue et al.* [1998] plot but are off-set by about $-2 R_E$. Approximately
276 11% of the data fall below a B_z value of less than -4nT .

277 With the P_d parameter, there is some small dependence of the radial difference for the
278 *Petrinec and Russell* [1996] model. At larger P_d , the radial differences for the *Petrinec and*
279 *Russell* [1996] model increase, however, the opposite is true for the other three models. As
280 P_d increases, the radial differences decrease for the *Shue et al.* [1998] model and become
281 increasingly negative for the *Dmitriev and Suvorova* [2000] and *Lin et al.* [2010] models.

282 The spacecraft angle, θ , has a small influence on the radial difference, with increasing
283 radial differences at increasing spacecraft angles (i.e. at high latitudes), for both the
284 *Petrinec and Russell* [1996] and *Shue et al.* [1998] models. A more pronounced, but
285 opposite, effect is noticed with the *Dmitriev and Suvorova* [2000] model where increasing
286 spacecraft angle results in an increasingly negative radial difference. The radial differences
287 for the *Lin et al.* [2010] model do not seem to be affected by the spacecraft angle.

288 The primary aim of this study was to as to use an automated routine, rather than
289 manual inspection, to determine crossing events and then compare these events to the
290 magnetopause models. However, to ensure that the results presented are statistically
291 valid, and not the product of an erroneous automated routine, we conducted a sample
292 study on the results. A random sample totalling 20% of the data was manually analyzed
293 and any false crossing identification events were removed. Of the 528 random events, 341
294 were identified as accurate crossing events. These were then plotted and compared to the
295 main plots and we found similar distributions for all; see Figure 8 for the comparison of
296 the medians from the full population and from the sample.

297 On inspection of those events where the routine had identified a crossing yet no such
298 crossing had occurred, we found that most events had only just qualified under our cri-
299 teria. Increasing the magnitude of the discontinuity in the magnetic field data required
300 to determine a crossing would help eliminate these false positives further but would also
301 severely impact the total number of accurate magnetopause crossing detections.

5. Summary

302 In this investigation, we created a more generalized version of the *Ivchenko et al.* [2000]
303 magnetopause crossing detection routine to explore its application at higher latitudes.
304 After applying our modified criteria to 8 years of Cluster magnetic field data we have
305 identified 2709 crossings of which we were able to compare 2640 crossings to four models:
306 two commonly used 2-D empirical models, one 3-D ANN model and one asymmetric
307 empirical 3-D model.

308 We find that the two empirical 2-D models, *Petrinec and Russell* [1996] and *Shue*
309 *et al.* [1998], generally agree well with each other. They both produce similar median
310 differences and interquartile ranges, when compared to our detected crossing locations,
311 though this is perhaps not unexpected since when *Shue et al.* [1998] compared their model
312 with that of *Petrinec and Russell* [1996] they found that the two models generally correctly
313 predicted dayside magnetopause crossings (the major differences occurring in the flanks).
314 Additionally, both models were developed using very similar datasets and so one might
315 expect similar results when using these models.

316 The radial differences between the detected crossing locations and the *Petrinec and*
317 *Russell* [1996] and *Shue et al.* [1998] modeled locations are off-set about a median of just
318 over 1 R_E . This indicates that, in general, the models over-estimate the radial distance

319 to the magnetopause (by about 9%). There are a couple of reasons for why this may be
320 the case. Firstly, the vast majority of the data in their crossing databases were obtained
321 using near-equatorial satellite missions (ISEE-1 & 2). It is now well known that, under
322 the same external conditions, the magnetopause is greater in size in the equatorial plane
323 than in the meridional plane [*Dmitriev and Suvorova*, 2000]. Since these two models were
324 based on low-latitude satellite missions, at middle latitudes where the magnetopause is
325 flatter, they would tend to overestimate the distance to the magnetopause.

326 This assumption is strengthened when the differences between the modeled magne-
327 topause locations of *Petrinec and Russell* [1996] and *Shue et al.* [1998] and the detected
328 locations are compared with the spacecraft angle. The models agreed well with the de-
329 tected locations at spacecraft angles (θ) of $< 40^\circ$ but there was an increase in the difference
330 at angles larger than this.

331 Secondly, the majority of the ISEE 1 & 2 data was collected during a period of of
332 rising solar activity (1977-1979) which resulted in an increased frequency of co-rotating
333 high-speed solar wind streams. The trailing edges of such solar wind streams are often
334 accompanied by regions of quasi-radial IMF and it has been shown that, in such conditions,
335 the magnetopause is expanded beyond its normal location [*Suvorova et al.*, 2010]. Hence,
336 in the case of *Petrinec and Russell* [1996] and *Shue et al.* [1998], who used large amounts
337 of data from this period to build their models, we should expect that the models will
338 overestimate the distance to the magnetopause during normal IMF conditions.

339 There was a clear trend in the radial difference between the detected location and the
340 modeled locations of *Shue et al.* [1998], *Dmitriev and Suvorova* [2000] and *Lin et al.* [2010]
341 when compared with solar wind dynamic pressure. For *Shue et al.* [1998], the differences

342 range from a median of $2 R_E$ at $P_d < 1$ nPa through to $-2 R_E$ at $P_d = 8$ nPa, with
343 $0 R_E$ occurring at around 4 nPa. The results of this plot closely match those of *Dušík et*
344 *al.* [2010] who compared 6649 THEMIS magnetopause crossings to the *Shue et al.* [1998]
345 model, though we compare crossings over a much wider range of latitudes. For *Dmitriev*
346 *and Suvorova* [2000] and *Lin et al.* [2010], there was similar trend to *Shue et al.* [1998] but
347 the data was distributed approximately $-2 R_E$ from the *Shue et al.* [1998] distribution.

348 The median difference between the predicted and measured location of the magne-
349 topause for the *Dmitriev and Suvorova* [2000] and *Lin et al.* [2010] models both suggest
350 that the models underestimate the radial distance to the magnetopause by $0.52 R_E$ and
351 $0.24 R_E$ respectively whereas the other two models overestimate it: by $1.06 R_E$ for *Petrinec*
352 *and Russell* [1996] and by $1.48 R_E$ for *Shue et al.* [1998].

353 As with many automated routines, we acknowledge that the modified *Ivchenko et al.*
354 [2000] routine used in this study will not identify all crossings and that it may determine
355 a crossing when no such event occurred. It does, however, provide a statistically valid
356 approach to detecting crossings with a large-scale data set.

357 The *Ivchenko et al.* [2000] crossing criteria, and our modified version of them, are based
358 purely on magnetic field data. Whilst this is convenient, since magnetic field data is the
359 most commonly available, straightforward and reliable data set, it is well known that
360 there are clear differences in the plasma characteristics between the magnetosheath and
361 magnetosphere regimes. Indeed, some studies (e.g. *Hapgood and Bryant* [1990]) primarily
362 use the plasma characteristics as the defining data set for determination of magnetopause
363 crossings. Incorporation of plasma data criteria into the modified *Ivchenko et al.* [2000]
364 crossing criteria requires further investigation.

365 In addition, we have used magnetic field data from the Cluster mission to determine
366 the magnetopause location since the spacecraft encountered the magnetopause at varying
367 magnetic latitude and local time. This was an improvement on other magnetopause
368 studies, whose spacecraft often visited similar regions of space. Nevertheless combining
369 data from multiple spacecraft missions, to increase spatial and temporal coverage, may
370 prove to be a useful future exercise.

371 **Acknowledgments.** We gratefully acknowledge the NASA/GSFC Space Physics Data
372 Facility's OMNIWeb service. We also acknowledge the Cluster Active Archive data facility
373 and the Cluster FGM team for the use of the Cluster data. NAC is supported by an STFC
374 studentship.

References

- 375 Berchem, J., and C. T. Russell (1982), The Thickness of the Magnetopause Current Layer:
376 ISEE 1 and 2 Observations, *J. Geophys. Res.*, *87*, A4, 2108–2114.
- 377 Chapman, S., and V. C. A. Ferraro (1931), A new theory of magnetic storm, I, The initial
378 phase, *J. Geophys. Res.*, *36*, 77
- 379 Dmitriev, A. V., and A. V. Suvorova (2000), Three-dimensional artificial neural net-
380 work model of the dayside magnetopause, *J. Geophys. Res.*, *105*(A8), 18909–18918,
381 doi:10.1029/2000JA900008.
- 382 Dmitriev, A. V., Suvorova, A. V., J.-K. Chao (2011), A predictive model
383 of geosynchronous magnetopause crossings, *J. Geophys. Res.*, *116*, A05208,
384 doi:10.1029/2010JA016208

- 385 Dušík, Š., G. Granko, J. Šafránková, Z. Němeček and K. Jelínek (2010), IMF cone angle
386 control of the magnetopause location: Statistical study, *Geophys. Res. Lett*, *37*, L19103,
387 doi:10.1029/2010GL044965.
- 388 Fairfield, D. H. (1971), Average and unusual locations of the Earth's magnetopause and
389 bow shock, *J. Geophys. Res.*, *78*, 23, 6700–6716
- 390 Gloag, J. M., E. A. Lucek, L.-N. Alconcel, A. Balogh, P. Brown, C. M. Carr, C. N.
391 Dunford, T. Oddy and J. Soucek (2010), FGM Data Products in the CAA, in *The*
392 *Cluster Active Archive*, edited by H. Laakso, M. Taylor and C. Escoubet, Astrophysics
393 and Space Science Proceedings, 109–128, Springer Netherlands, doi:10.1007/978-90-481-
394 3499-1_7
- 395 Hapgood, M. A., T. G. Dimbylow, D. C. Sutcliffe, P. A. Chaizy, P. S. Ferron, P. M. Hill
396 and X. Y. Tiratay (1997), The Joint Science Operations Centre, *Space Sci. Rev.*, *79*,
397 487–525
- 398 Hapgood, M. A., and D. A. Bryant (1990), Re-ordered electron data in the low-latitude
399 boundary layer, *Geophys. Res. Lett*, *17*, 2043–2046
- 400 Ivchenko, N. V., D. G. Sibeck, K. Takahashi and S. Kokubun (2000), A statistical study
401 of the magnetosphere boundary crossings by the Geotail satellite, *Geophys. Res. Lett*,
402 *27*, 18, 2881–2884
- 403 Khan, H. and S. W. H. Cowley (1999), Observations of the response time of high-latitude
404 ionospheric convection to variations in the interplanetary magnetic field using EISCAT
405 and IMP-8 data, *Ann. Geophys.*, *17*, 1306–1335
- 406 Kuznetsov, S. N., and A. V. Suvorova (1997), Magnetopause shape near geosynchronous
407 orbit (in Russian), *Geomagn. Aeron*, *37*(3), 1–11

- 408 Laakso, H., M. Taylor and C. P. Escoubet (Eds.) (2010), *The Cluster Active Archive*,
409 Astrophysics and Space Science Proceedings, Springer New York
- 410 Lin, R. L., X. X. Zhang, S. Q. Liu, Y. L. Wang, and J. C. Gong (2010), A three-dimensional
411 asymmetric magnetopause model, *J. Geophys. Res.*, *115*, doi:10.1029/2009JA014235
- 412 Nishida, A. (1994), The GEOTAIL Mission, *Geophys. Res. Lett.*, *21*, 25, 2871–2873,
413 doi:10.1029/94GL01223
- 414 Petrinec, S. M., and C. T. Russell (1993), An empirical model of the size and shape of
415 the near-Earth magnetotail, *Geophys. Res. Lett.*, *20*, 2695
- 416 Petrinec, S. M., and C. T. Russell (1996), Near-Earth magnetotail shape and size as
417 determined from the magnetopause flaring angle, *J. Geophys. Res.*, *101*(A1), 137–152
- 418 Petrinec, S. M., P. Song, and C. T. Russell (1991), Solar cycle variation in the size and
419 shape of the magnetopause, *J. Geophys. Res.*, *96*, 78936-7896
- 420 Roelof, E. C. and D. G. Sibeck (1993), Magnetopause shape as a bivariate function of
421 interplanetary magnetic field B_z and solar wind dynamic pressure, *J. Geophys. Res.*,
422 *98*, 21421-21450, doi:10.1029/93JA02362
- 423 Šafránková, J., Z. Němeček, Š. Dušík, L. Přech, D. G. Sibeck, and N. N. Borodkova
424 (2002), The magnetopause shape and location: a comparison of the Interball and Geotail
425 observations with models, *Ann. Geophys.*, *20*, 301–309
- 426 Shue, J. H., J. K. Chao, H. C. Fu, C. T. Russell, P. Song, K. K. Khurana and H. J. Singer
427 (1997), A new functional form to study the solar wind control of the magnetopause size
428 and shape, *J. Geophys. Res.*, *102*, 9497–9511
- 429 Shue, J.-H., P. Song, C. T. Russell, J. T. Steinberg, J. K. Chao, G. Zastenker, O. L. Vais-
430 berg, S. Kokubun, H. J. Singer, T. R. Detman and H. Kawano (1998), Magnetopause

- 431 location under extreme solar wind conditions, *J. Geophys. Res.*, *103*(A8), 17691–17700,
432 doi:10.1029/98JA01103
- 433 Sibeck, D. G., R. E. Lopez, and E. C. Roelof (1991), Solar wind control of the
434 magnetopause shape, location, and motion, *J. Geophys. Res.*, *96*(A4), 5489-5495,
435 doi:10.1029/90JA02464
- 436 Song, P., R. C. Elphic and C. T. Russell (1988), ISEE 1 and 2 observations of the oscillating
437 magnetopause, *Geophys. Res. Lett.*, *15*, 744
- 438 Suvorova A.V, A.V. Dmitriev, S.N. Kuznetsov (1999), Dayside magnetopause models,
439 *Rad. Meas.*, *30*(5), 687–692.
- 440 Suvorova, A. V., J.-H. Shue, A. V. Dmitriev, D. Sibeck, J. McFadden, H. Hasegawa,
441 K. Ackerson, K. Jelinek, J. Safrankova, Z. Nemecek (2010), Magnetopause expansions
442 for quasi-radial interplanetary magnetic field: THEMIS and Geotail observations, *J.*
443 *Geophys. Res.*, *115*, A10216, doi:10.1029/2010JA015404.
- 444 Wild, J. A., E. E. Woodfield and S. K. Morley (2009), On the triggering of auroral
445 substorms by northward turnings of the interplanetary magnetic field, *Ann. Geophys.*,
446 *27*(9), 3559–3570, doi:10.5194/angeo-27-3559-2009

Figure 1. An example of the plots produced by the crossing detection routine. The three panels on the left of the figure present the magnetic field data (the magnetic field strength $|B|$ (black) and chosen magnetic field component which is B_r in this case (purple), the running standard deviation of a three minute segment of the magnetic field strength, and the clock angle (measured with Cluster in blue and predicted by OMNIweb in yellow). The red dashed line indicates a detected inward crossing; the black dashed line indicates the time the spacecraft were

D R A F T

September 11, 2013, 11:27am

D R A F T

predicted to cross the magnetopause. The panel on the right shows the spacecraft position and

a modeled magnetosphere for the time of the crossing (in GSE co-ordinates).

Figure 2. A density plot of detected magnetopause crossings locations in GSM co-ordinates. Position ρ is defined as $\sqrt{Y_{GSM}^2 + Z_{GSM}^2}$ (see equation 3 for further details). The density of each bin is represented by the logarithmic color scale.

Figure 3. A histogram of the radial differences, as calculated in equation 1, between the detected crossing location and the *Petrinec and Russell* [1996] modeled magnetopause location. The three vertical dashed blue lines represent the lower interquartile, the median and the upper interquartile respectively.

Figure 4. A histogram, of the same form as Figure 3, for the *Shue et al.* [1998] model.

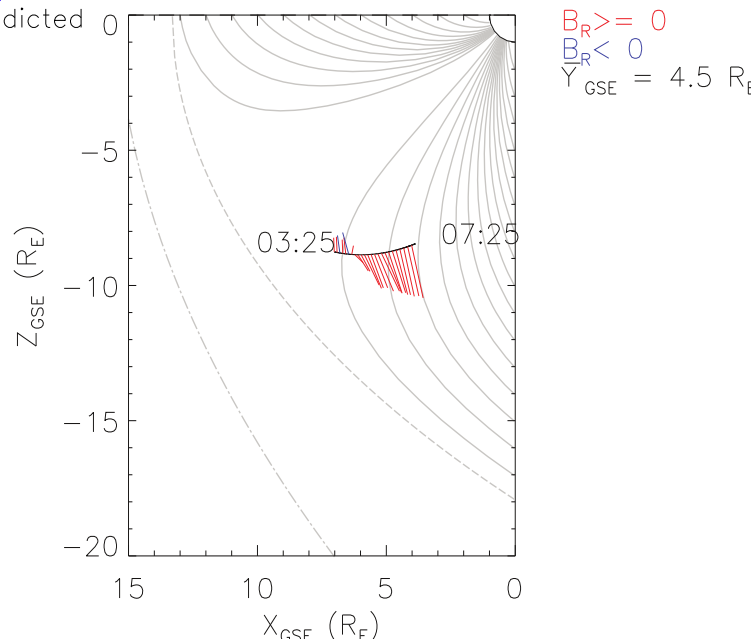
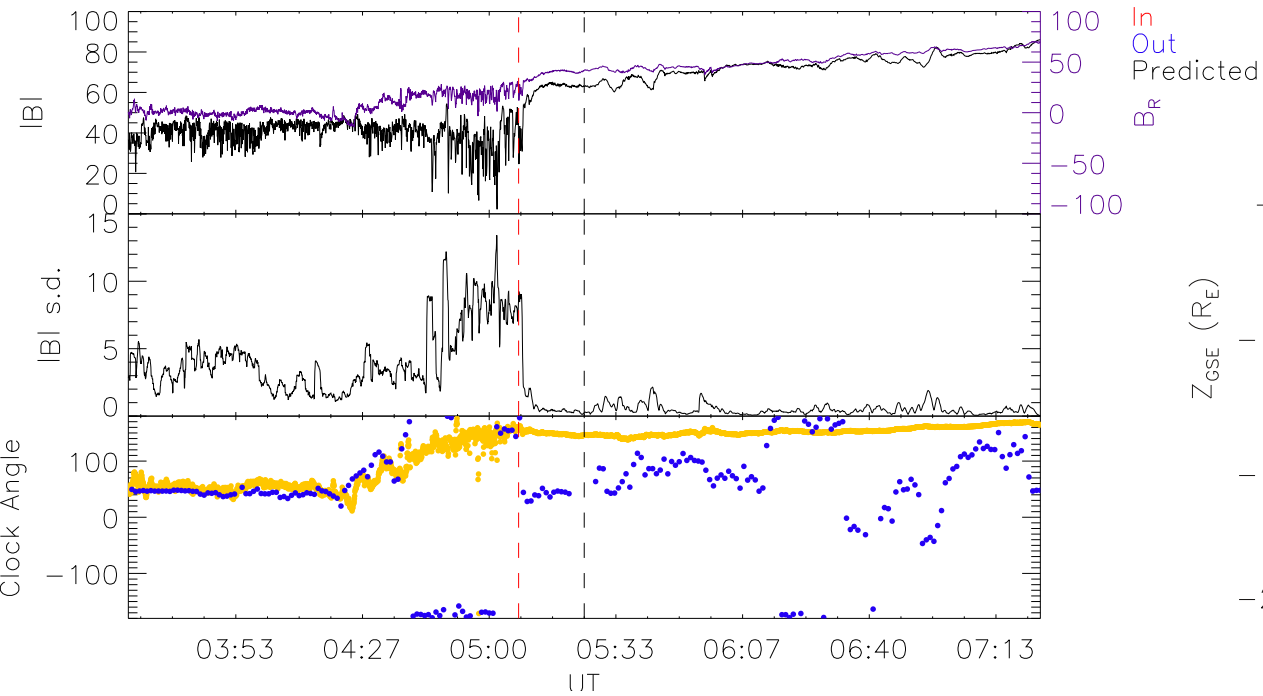
Figure 5. A histogram, of the same form as Figure 3, for the *Dmitriev and Suvorova* [2000] model.

Figure 6. A histogram, of the same form as Figure 3, for the *Lin et al.* [2010] model.

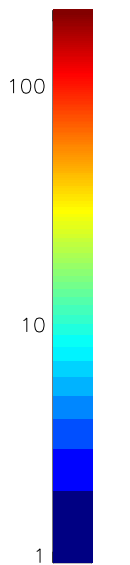
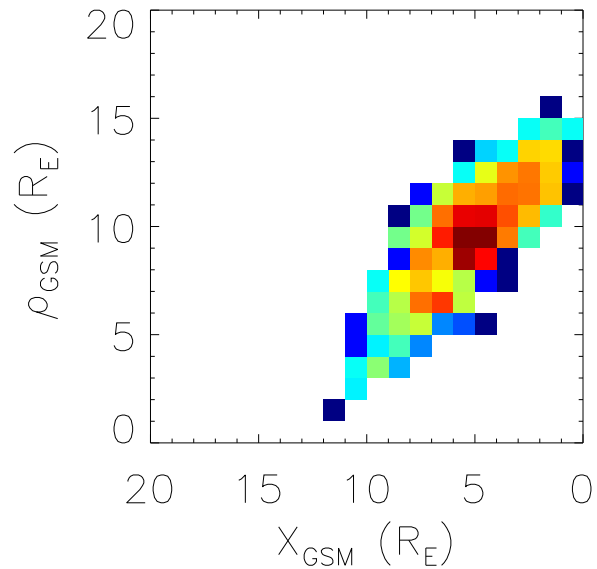
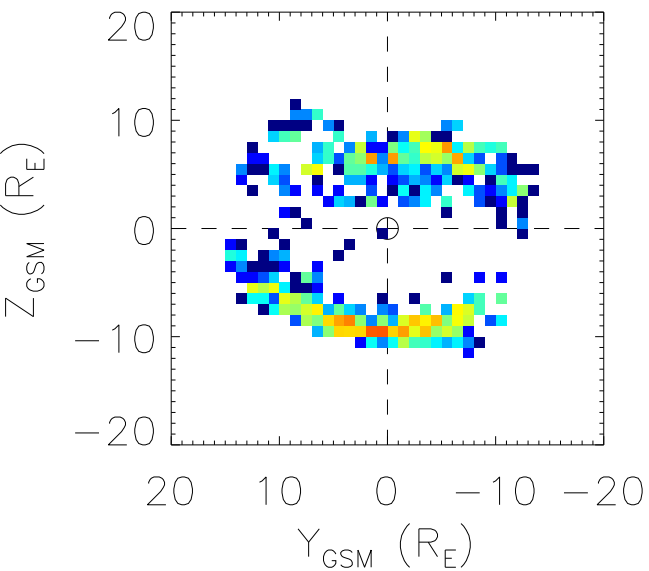
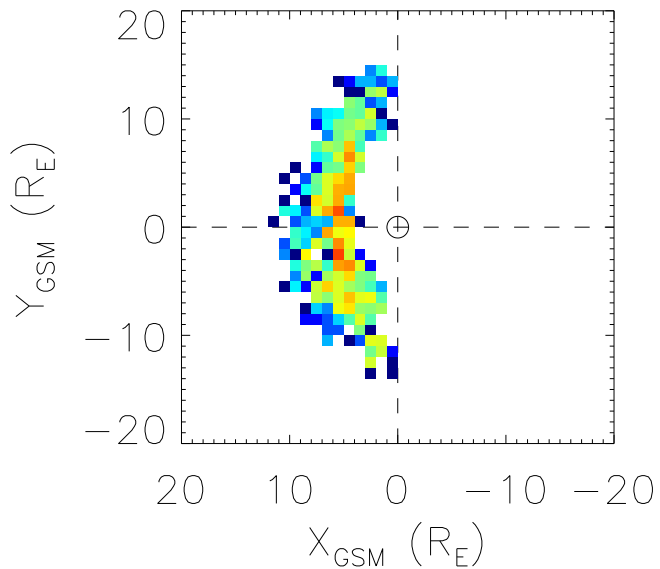
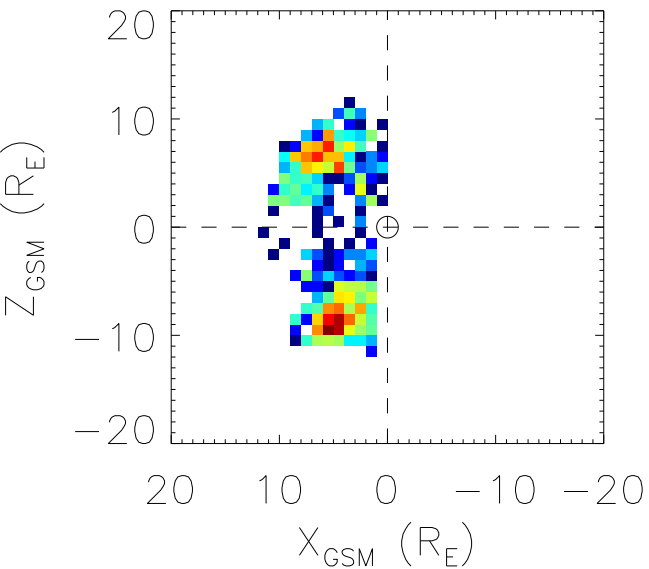
Figure 7. A comparison of the radial difference between the detected magnetopause location and the modeled locations for each of the three models, plotted for the four parameters (clock angle, B_z , P_d and spacecraft angle θ). The density of the bins is represented by the logarithmic color bar. The median radial difference for each row is denoted by the cross and the error bars represent the interquartile range of the row.

Figure 8. A comparison of the medians for the full population (blue) and the 20% sample (red), plotted again for the four parameters (clock angle, B_z , P_d and spacecraft angle θ). The solid lines indicate the median value for the row and the lightly shaded areas represent the interquartile range of each row.

2004/01/06 - Sc1 - I

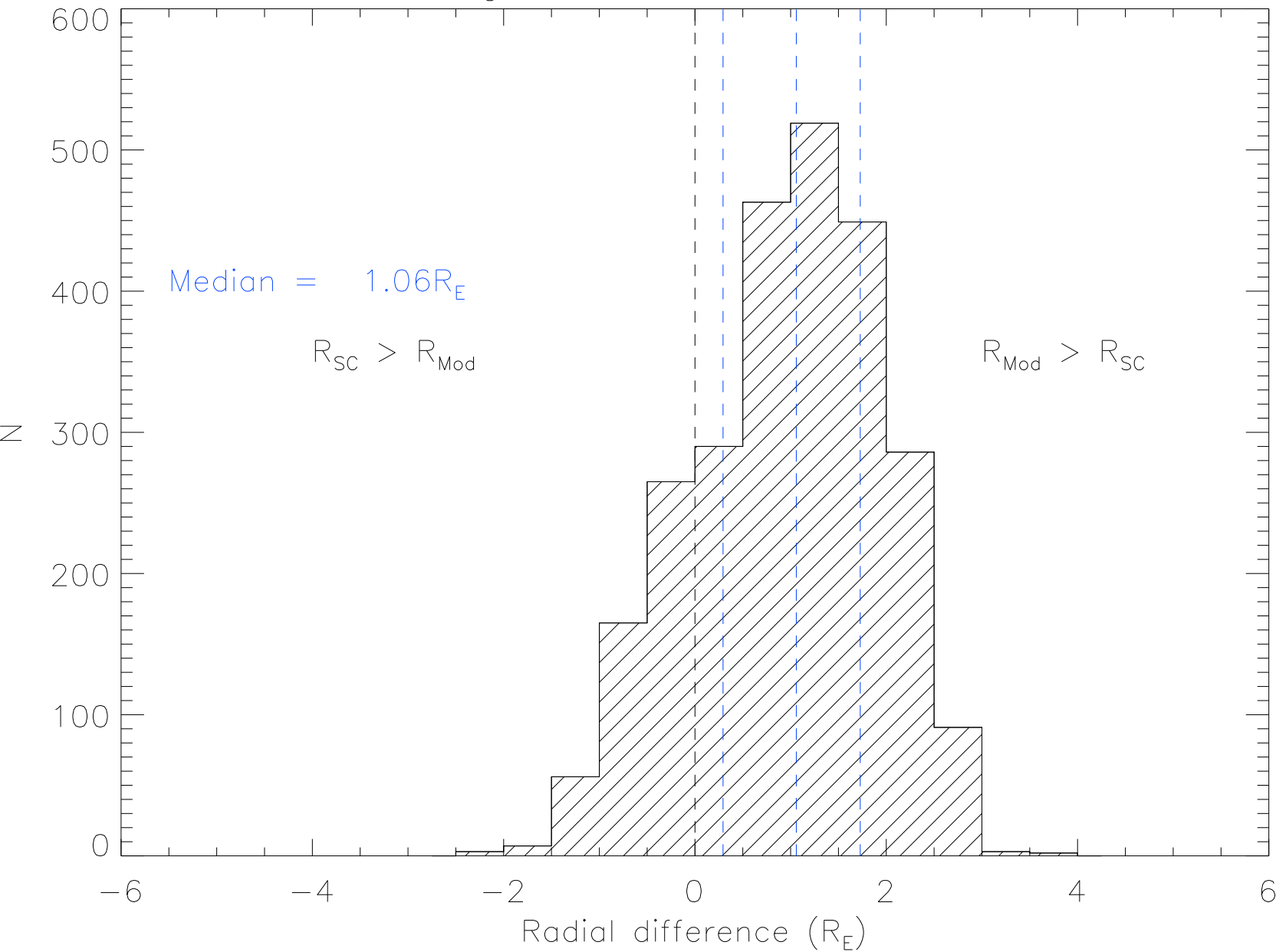


Detected crossing locations

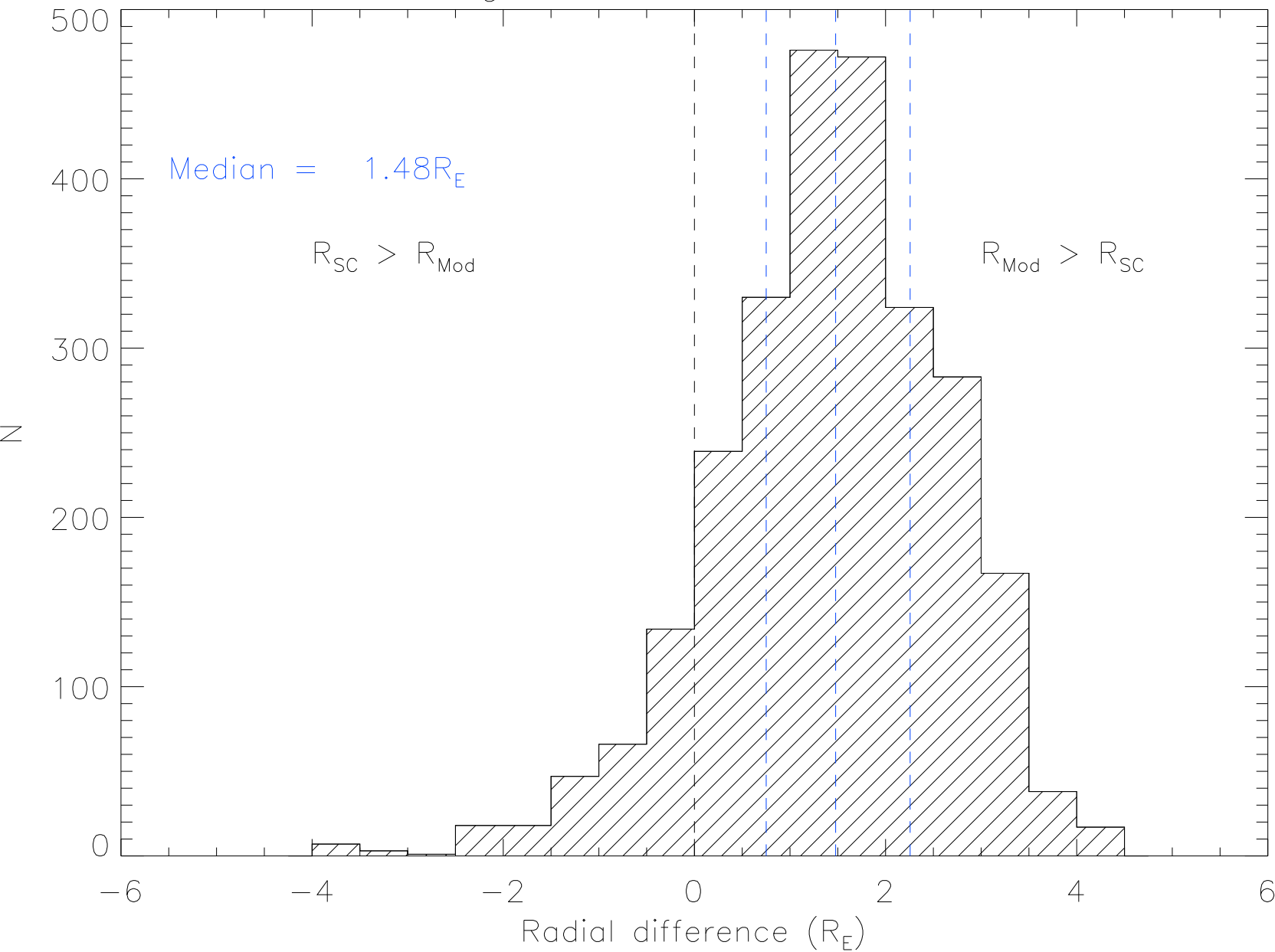


Bin density

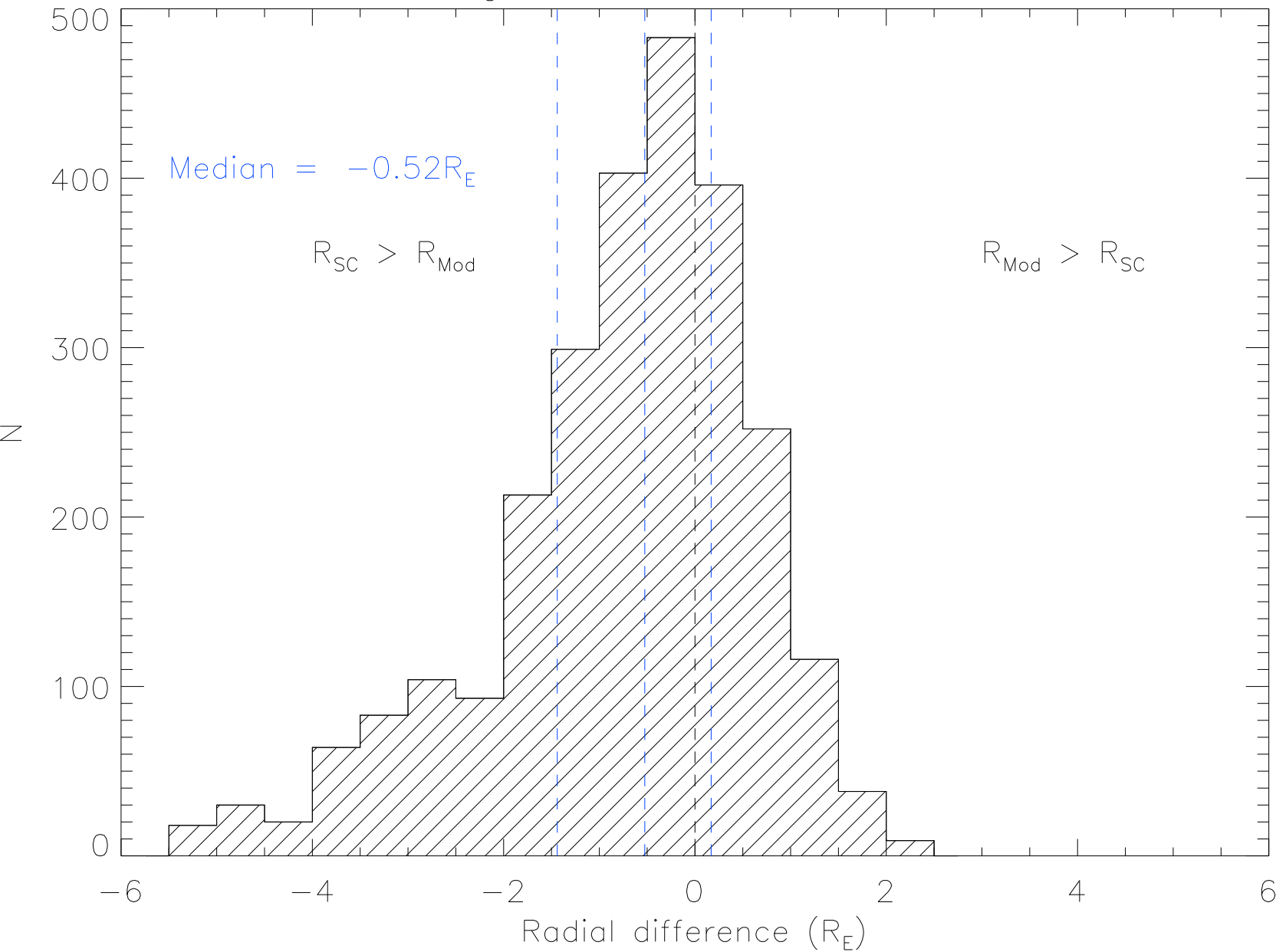
Histogram of radial differences



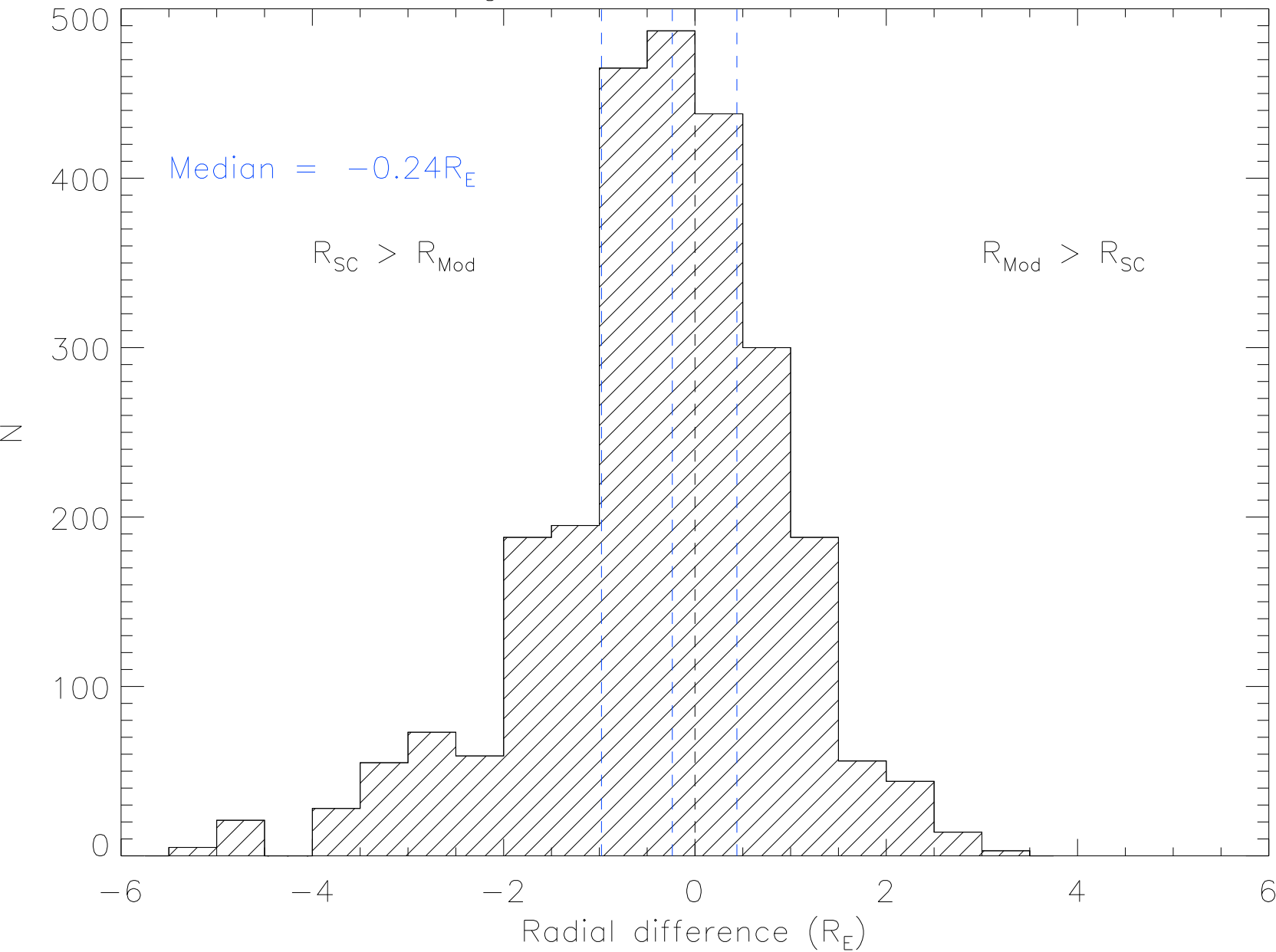
Histogram of radial differences



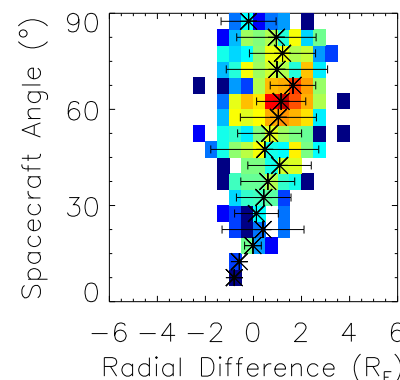
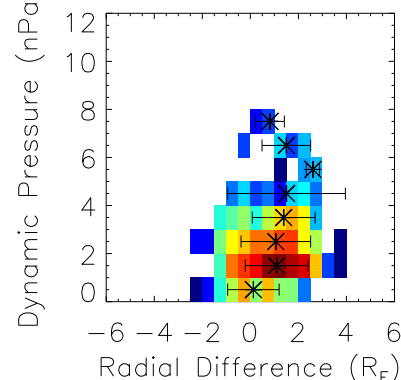
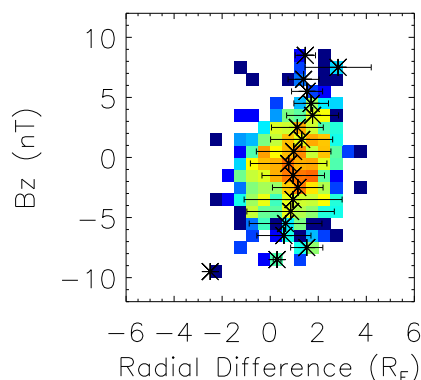
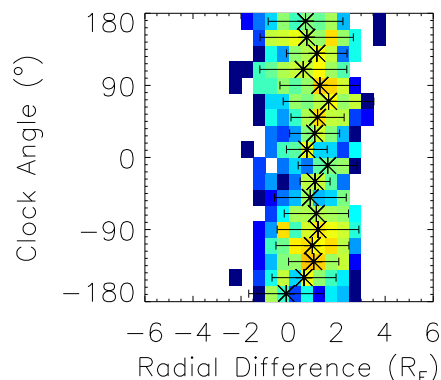
Histogram of radial differences



Histogram of radial differences

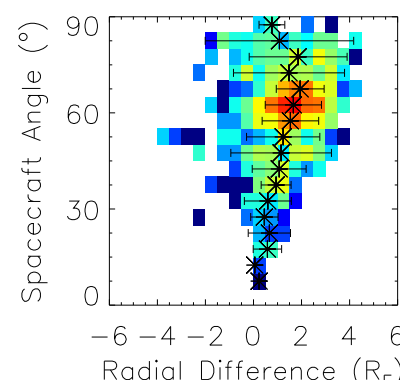
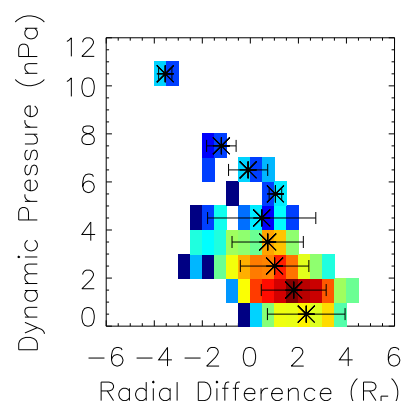
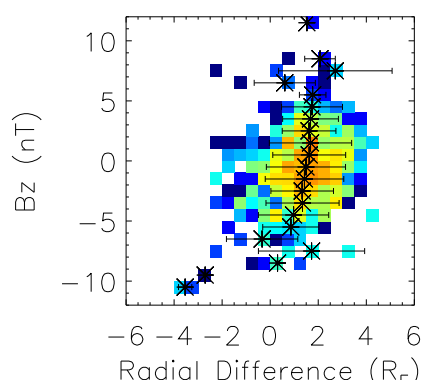
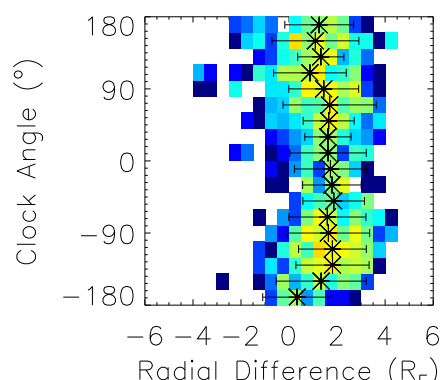


Petrinec and Russell



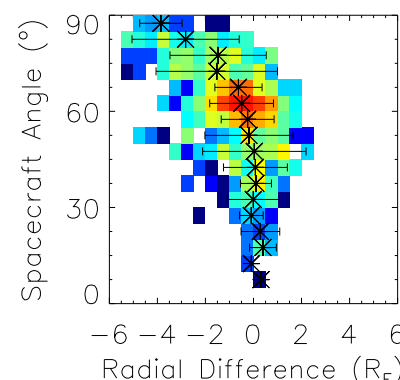
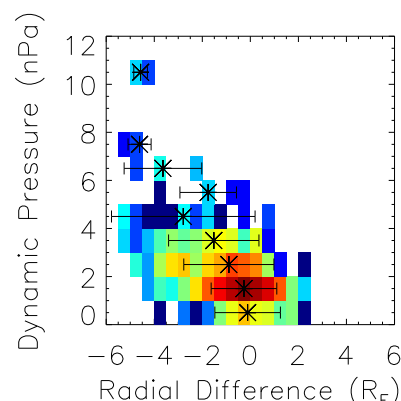
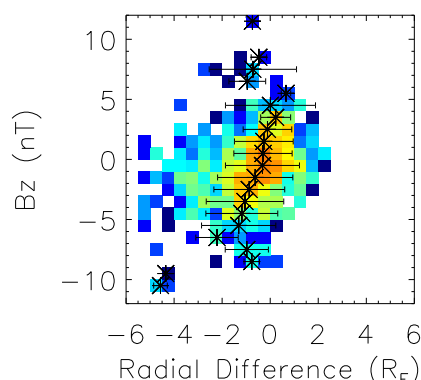
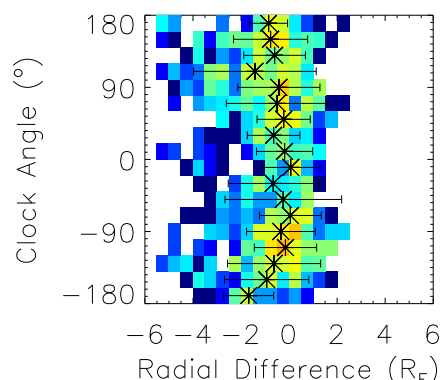
Bin density

Shue et al.



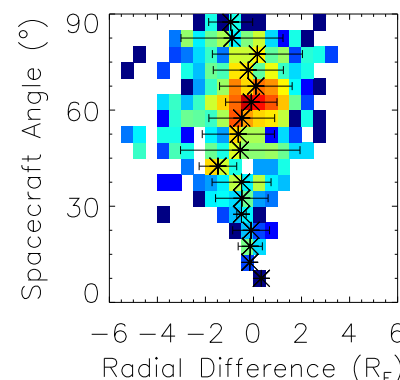
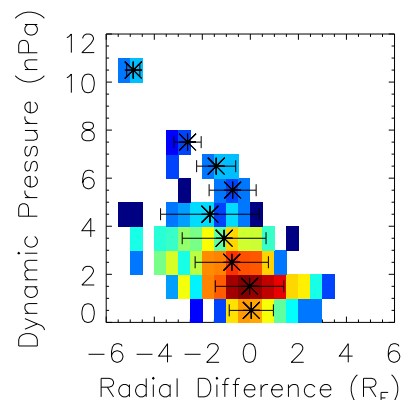
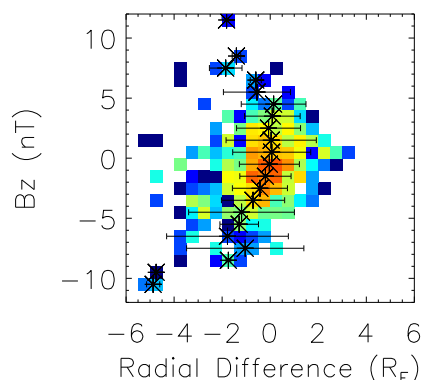
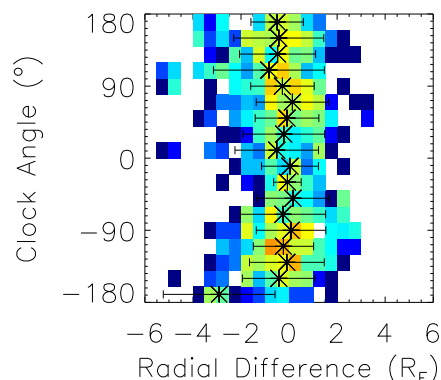
Bin density

Dmitriev & Suvorova



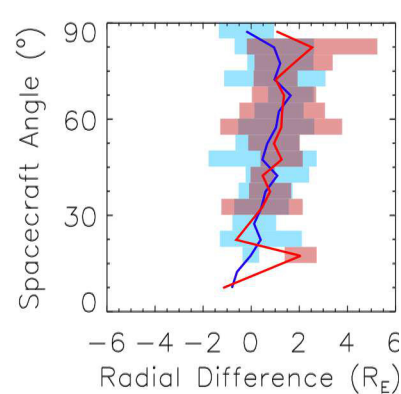
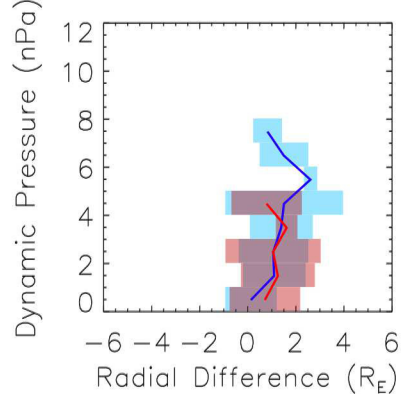
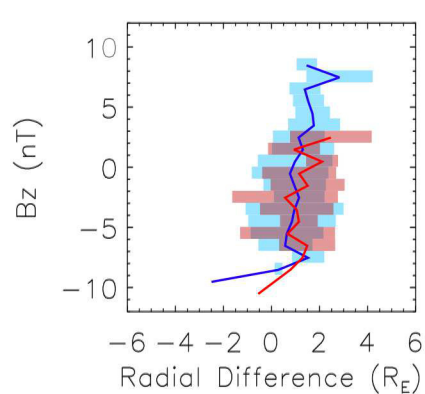
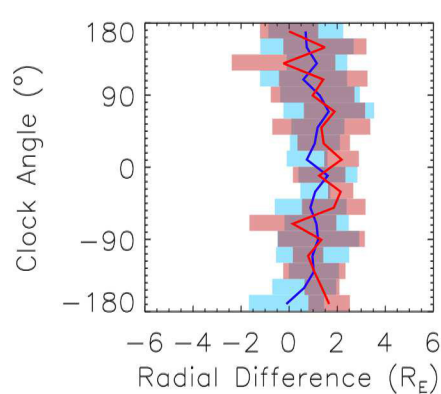
Bin density

Lin et al.

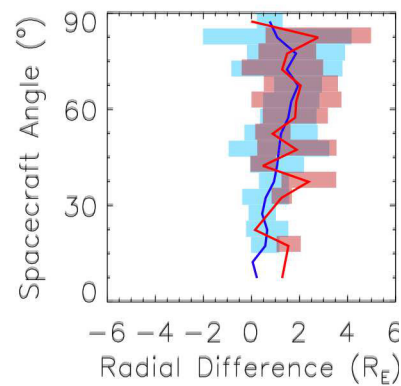
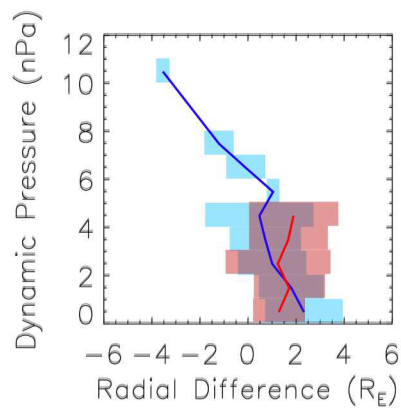
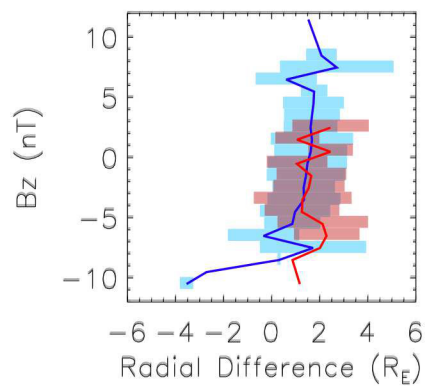
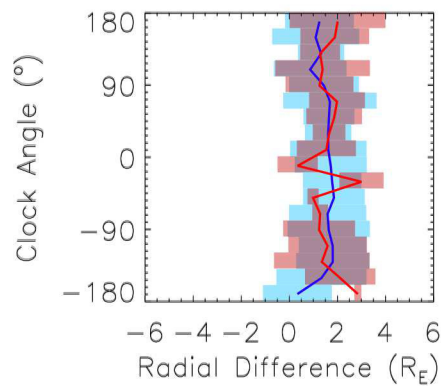


Bin density

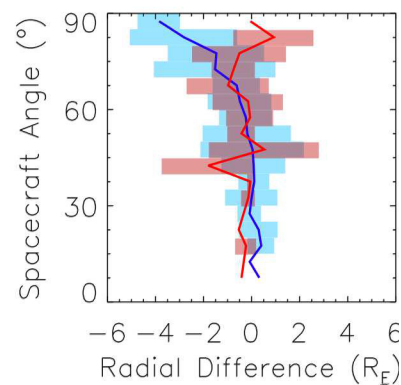
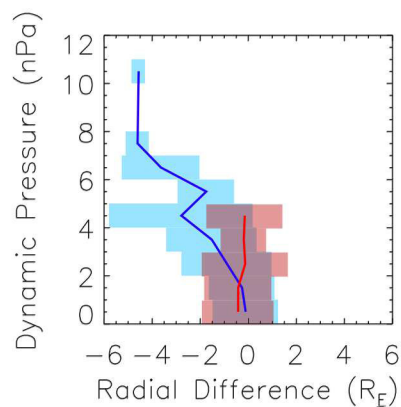
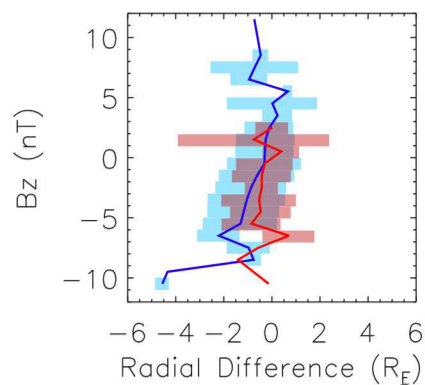
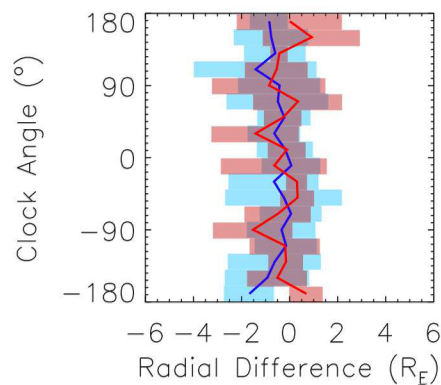
Petrinec and Russell



Shue et al.



Dmitriev & Suvorova



Lin et al.

